Inorg. Chem. **2003**, *42*, 140–147

Light-Induced Metastable Linkage Isomers of Ruthenium Sulfur Dioxide Complexes

Andrey Yu. Kovalevsky,[†] Kimberly A. Bagley,[‡] Jacqueline M. Cole,[†,§] and Philip Coppens*[,†]

Chemistry Department, University at Buffalo, The State University of New York at Buffalo, Buffalo, New York 14260, and Department of Chemistry, State University College of New York at Buffalo, Buffalo, New York 14222

Received September 3, 2002

The irradiation of ruthenium–sulfur dioxide complexes of general formula *trans*-[$Ru^{II}(NH_3)_4(SO_2)X$]Y with laser light at low temperature results in linkage isomerization of SO_2, starting with η^1-planar *S*-bound to η^2-side *S*,*O*-bound SO_2. The solid-state photoreaction proceeds with retention of sample crystallinity. Following work on *trans*-[$Ru(NH_3)_4Cl(\eta^1\text{-}SO_2)$]Cl and *trans*-[$Ru(NH_3)_4(H_2O)(\eta^1\text{-}SO2)](C_6H_5SO_3)_2$ (Kovalevsky, A. Y.; Bagley, K. A.; Coppens, P. *J. Am. Chem. Soc.* **2002**, *124*, 9241–9248), we describe photocrystallographic, IR, DSC, and theoretical studies of *trans*-[$Ru^{II}(NH_3)_4(SO_2)X$]Y complexes with (X = Cl^-, H_2O, or CF_3COO^- (TFA^-)) and a number of different counterions (Y = Cl^-, $C_6H_5SO_3^-$, Tos^-, or TFA^-). Low temperature IR experiments indicate the frequency of the asymmetric and symmetric stretching vibrations of the Ru-coordinated SO_2 to be downshifted by about 100 and 165 cm^{-1}, respectively. Variation of the trans-to-SO_2 ligand and the counterion increases the MS2 decay temperature from 230 K (*trans*-[$Ru^{II}(NH_3)_4(SO_2)Cl$]Cl) to 276 K (*trans*-[$Ru^{II}(NH_3)_4(SO_2)(H_2O)$]$(Tos)_2$). The stability of the MS2 state correlates with increasing σ-donating ability of the trans ligand and the size of the counterion. Quantum chemical DFT calculations indicate the existence of a third η^1-*O*-bound (MS1) isomer, the two metastable states being 0.1–0.6 eV above the energy of the ground-state complex.

Introduction

Photocrystallography is a developing technique, in which X-ray diffraction of laser-irradiated crystals is combined with spectroscopic and differential scanning calorimetry (DSC) measurements. The method was introduced in our laboratory for the study of the light-induced linkage isomers in transition metal nitrosyl complexes.[1] To study photoinduced metastable states, collection of "dark" data is followed by a "light" experiment on the same diffractometer-mounted crystal after exposure to light. Information from the two experiments is combined in the determination of the geometry of the light-induced species. In parallel, the IR spectrum of a sample (usually a KBr pellet) before and after irradiation is measured,[2−5] and the DSC of a previously irradiated crystalline sample, which releases energy during decay of the metastable state on warming, is recorded.[1,5−7]

Transition metal complexes containing the nitrosyl ligand (NO) were the first series of compounds investigated systematically. Upon irradiation, nitrosyl undergoes linkage isomerization from almost linear *N*-bound in the ground state to iso-η^1-*O*-bound (MS1) and to η^2-*N*,*O*-side-bound (MS2) configurations, as summarized elsewhere.[8]

In a previous publication, we identified photoinduced linkage isomers of *trans*-[$Ru(NH_3)_4Cl(\eta^1\text{-}SO_2)$]Cl (**1**) and *trans*-[$Ru(NH_3)_4(H_2O)(\eta^1\text{-}SO_2)](C_6H_5SO_3)_2$ (**2**)[9] and confirmed Johnson's and Dew's proposal, based on IR data evidence, of η^1-planar-*S*-bound to η^2-side-*S*,*O*-bound linkage isomerization of sulfur dioxide in the solid state.[10] In the

* To whom correspondence should be addressed. E-mail: coppens@acsu.buffalo.edu. Phone: (716) 645-6800 ext. 2217. Fax: (716) 645-6948.
† University at Buffalo, The State University of New York at Buffalo.
‡ State University College of New York at Buffalo.
§ Permanent address: Department of Chemistry, University of Cambridge, Lensfield Road, Cambridge, CB2 1EW U.K.

(1) Coppens, P.; Fomitchev, D. V.; Carducci, M. D.; Culp, K. *J. Chem. Soc., Dalton Trans.* **1998**, 865−872.
(2) Fomitchev, D. V.; Coppens, P.; Li, T.; Bagley, K. A.; Chen, L.; Richter-Addo, G. B. *Chem. Commun.* **1999**, 2013−2014.
(3) Chen, L.; Novozhilova, I.; Kim, C. D.; Kovalevsky, A. Yu.; Bagley, K. A.; Coppens, P.; Richter-Addo, G. B. *J. Am. Chem. Soc.* **2000**, *122*, 7142−7143.
(4) Kim, C. D.; Novozhilova, I.; Goodman, M. S.; Bagley, K. A.; Coppens, P. *Inorg. Chem.* **2000**, *39*, 5791−5795.
(5) Fomitchev, D. V.; Novozhilova, I.; Coppens, P. *Tetrahedron* **2000**, *56*, 6813−6820.
(6) Fomitchev, D. V.; Coppens, P. *Inorg. Chem.* **1996**, *35*, 7021−7026.
(7) Fomitchev, D. V.; Coppens, P. *Comments Inorg. Chem.* **1999**, *21* (1−3), 131−148.
(8) Coppens, P.; Novozhilova, I. V.; Kovalevsky, A. Y. *Chem. Rev.* **2002**, *102*, 861−884.

10.1021/ic025997g CCC: $25.00
Published on Web 12/10/2002

terminology used for the nitrosyl linkage isomers, the photoinduced species represent MS2 metastable states, which return back to the ground state upon warming following low-temperature illumination of the samples. The MS2 states of the two complexes differ in the details of their geometry in the Ru−SO_2 region.

We report here combined photocrystallographic, spectroscopic, and theoretical studies of linkage isomers of a number of additional ruthenium sulfur dioxide complexes, of general formula *trans*-[$Ru^{II}(NH_3)_4(SO_2)X$]Y, where X is the ligand trans-to-SO_2 (Cl^-, H_2O, or CF_3COO^- (trifluoroacetic acid, TFA^-)), and Y the counterion (Cl^-, $C_6H_5SO_3^-$, Tos^-, or TFA^-), performed to further explore the geometry and relative stability of the photoinduced species.

Sulfur dioxide is a most versatile ligand.[11,12] Its coordination modes range from η^1-planar *S*-bound and η^1-pyramidal *S*-bound to η^2-side-*S*,*O*-bound and η^1-*O*-bound configurations. Complexes incorporating these binding modes have been synthesized, and several have been structurally characterized.[11,13,14] Only two examples of stable ruthenium complexes containing η^2-*S*,*O*-bound sulfur dioxide are known.[15,16] Both are trigonal bipyramidal complexes of Ru^0. In addition to the photoinduced metastable isomer of [$Ru^{II}(NH_3)_4Cl(\eta^1$-$SO_2)$]Cl, proposed by Johnson and Dew,[10] Kubas et al.[17] concluded, on the basis of IR evidence, that the *fac*-$Mo(CO)_3$(dppe)(η^2-SO_2) complex spontaneously rearranges in solution to give the mer isomer, in which SO_2 adopts an η^1-*S*-bound planar geometry.

Experimental Section

Preparation of the Ruthenium Complexes. Materials. Regular distilled water was used in all preparations. Sulfur dioxide gas and tetrafluoroboric (HBF_4), toluenesulfonic, and trifluoroacetic (HTFA) acids were purchased from Aldrich, and used without further purification.

***trans*-Tetraamminechloro(sulfur dioxide)ruthenium(II) Tetrafluoroborate (3).** *trans*-[$Ru(NH_3)_4Cl(SO_2)$]Cl (50 mg) was added to the hot solution of 5 mL of 75% HBF_4 acid. After the solid was dissolved, the clear orange solution was stirred for about 10 min, filtered while hot, and put aside for several days. Fine bricklike orange crystals appeared, which were filtered on a frit, washed with Et_2O, and air-dried to give 40 mg (≈70% yield) of *trans*-[$Ru(NH_3)_4Cl(SO_2)$](BF_4) (**3**). A small crystal suitable for X-ray analysis was selected from the obtained solid.

***trans*-Tetraammineaquo(sulfur dioxide)ruthenium(II) Tetrafluoroborate (4).** Freshly prepared *trans*-[$Ru(NH_3)_4(HSO_3)_2$] (50 mg), an intermediate in the preparation of *trans*-[$Ru(NH_3)_4Cl(SO_2)$]-Cl, was dissolved in 5 mL of 20% HBF_4 acid in a small beaker. The solid dissolved quickly to form an orange solution, which was allowed to stand for a week in air at room temperature. During this time, orange crystals suitable for X-ray analysis formed. They were filtered on a frit, washed with Et_2O, and air-dried to give 57 mg (≈90% yield) of *trans*-[$Ru(NH_3)_4(H_2O)(SO_2)$](BF_4)$_2$ (**4**).

***trans*-Tetraammineaquo(sulfur dioxide)ruthenium(II) Tosylate (5).** Toluenesulfonic acid (0.2 g) was dissolved in 10 mL of water. To this solution was added 50 mg of *trans*-[$Ru(NH_3)_4Cl(SO_2)$]Cl and the mixture heated to about 90 °C under vigorous stirring. The solid dissolved within several minutes. The resulting clear yellow-brown solution was cooled to room temperature. Large yellow-orange platelike crystals appeared within a day. They were treated in the same way as compound **3** to give a quantitative yield of *trans*-[$Ru(NH_3)_4(H_2O)(SO_2)$](Tos)$_2$ (**5**). A brick-shaped crystal suitable for X-ray analysis was cut from a large plate.

***trans*-Tetraammine(trifluoroactate)(sulfur dioxide)ruthenium(II) Trifluoroacetate Trifluoroacetic Acid Solvate (1/1/1) (6).** To 50 mg of *trans*-[$Ru(NH_3)_4Cl(SO_2)$]Cl was added 4 mL of 50% HTFA. The resulting mixture was heated to approximately 80 °C for 15 min, while stirring vigorously. To remove undissolved solid, the deep orange solution was filtered while hot. It was cooled to room temperature and allowed to stand in air. Bright orange platelike crystals began to precipitate in about 10 days, after the solvent had almost evaporated. They were collected on a frit (23 mg, ≈40% yield), without washing, and stored under nitrogen because of their instability toward other solvents and air. A small brick-shaped crystal suitable for X-ray analysis was cut from a large plate.

Photocrystallography. X-ray diffraction data on **3**−**6** were collected at 90(1) K using a Bruker SMART1000 CCD diffractometer installed at a rotating anode source (Mo Kα radiation) and equipped with an Oxford Cryosystems nitrogen gas-flow apparatus. The data were collected by the rotation method with 0.3° frame width (ω scan) and 20 s exposure time per frame. For each experiment, four sets of data (600 frames in each set) were collected, nominally covering half of reciprocal space. The data were integrated, scaled, sorted, and averaged using the SMART software package.[18] The structures were solved by the Patterson method for **3** and **4**, and by direct methods for **5** and **6**, using SHELXTL NT Version 5.10.[19]

As the SO_2 groups in **3** and **4** are disordered over two positions, these complexes were not judged suitable for the photocrystallographic experiments but were included in other measurements. Crystals of **5** and **6** mounted on the diffractometer and cooled to 90 K were irradiated in situ with 488 nm light from Ar^+ CW laser for 10 and 2 min, respectively. During exposure, the crystals were continuously rotated around the diffractometer's φ angle to maximize the uniformity of irradiation. The rotation velocities were selected such that the crystals of **5** and **6** made two full 360° revolutions during the total exposure time. The laser output power was reduced to approximately 0.5 W for compound **5** and 0.38 W for compound **6** to minimize damage to the crystals. During the irradiation, the crystals darkened from orange to deep red-brown (Figure 1). Further irradiation resulted in weakening of the Bragg spots and the appearance of powder lines, indicating that, under the conditions selected, further conversion led to breakdown of the crystal matrix. In both cases, data collection was started after a delay of 10−20 min in order to dissipate any heat accumulated in the crystal during light exposure.

(9) Kovalevsky, A. Y.; Bagley, K. A.; Coppens, P. *J. Am. Chem. Soc.* **2002**, *124*, 9241−9248.
(10) Johnson, D. A.; Dew, V. C. *Inorg. Chem.* **1979**, *18*, 3273−3274.
(11) Ryan, R. R.; Kubas, G. J.; Moody, D. C.; Eller, P. G. *Struct. Bonding* (*Berlin*) **1981**, *46*, 48−100.
(12) Mingos, D. M. P. *Transition Met. Chem.* **1978**, *3*, 1−15.
(13) Mingos, D. M. P. *Transition Met. Chem.* **1978**, *3*, 1−15.
(14) Kubas, G. J. *Inorg. Chem.* **1979**, *18* (1), 182−188.
(15) Wilson, R. D.; Ibers, J. A. *Inorg. Chem.* **1978**, *17*, 2134−2138.
(16) Moody, D. C.; Ryan, R. R. *J. Chem. Soc., Chem. Commun.* **1980**, 1230−1231.
(17) Kubas, G. J.; Jarvinen, G. D.; Ryan, R. R. *J. Am. Chem. Soc.* **1983**, *105*, 1883−1891.
(18) *SMART and SAINTPLUS*; area detector control and integration software, version 6.01; Bruker AXS: Madison, WI, 1999.
(19) *SHELXTL*; an integrated system for solving, refining and displaying crystal structures from diffraction data, version 5.10; Bruker AXS: Madison, WI, 1997.

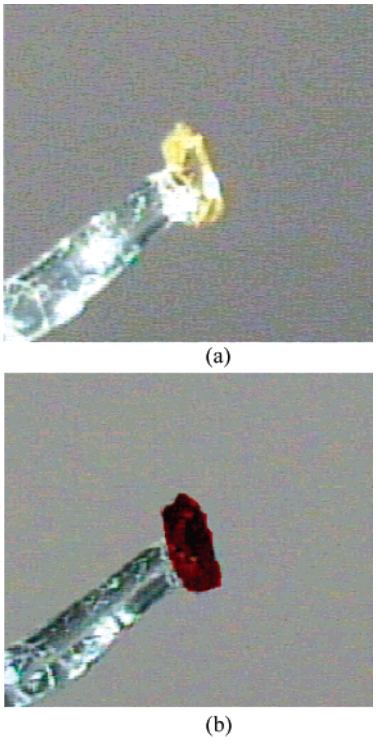

Figure 1. Color change of the crystal of **5** before (a) and after (b) irradiation with 488 nm laser light for 10 min.

Table 1. Crystallographic Data of "Dark" and "Light" Experiments for **5** and **6**[a]

	5		**6**	
	GS	MS2/GS	GS	MS2/GS
cryst shape	yellow-orange bricks	deep red-brown bricks	bright orange bricks	deep red-brown bricks
cryst syst	triclinic	triclinic	monoclinic	monoclinic
space group	$P\bar{1}$	$P\bar{1}$	Cc[b]	Cc
a [Å]	6.6769(2)	6.6558(3)	9.2938(4)	9.4520(3)
b [Å]	13.0777(3)	13.1033(6)	27.274(1)	27.4390(9)
c [Å]	13.6128(4)	13.6851(7)	7.0515(3)	6.9231(2)
α [deg]	94.445(1)	94.603(1)	90	90
β [deg]	92.840(1)	93.212(2)	104.073(1)	99.918(1)
γ [deg]	103.597(1)	103.366(1)	90	90
V [Å^3]	1149.04(5)	1154.02(9)	1733.7(1)	1768.7(1)
Z	2	2	4	4
ρ_{calcd} [g/cm^3]	1.716	1.708	2.197	2.153
μ [mm^{-1}]	1.007	1.003	1.165	1.142
T [K]	90(1)	90(1)	90(1)	90(1)
max 2θ [deg]	60.00	50.02	60.08	60.06
abs correction method	SADABS[18]	SADABS[18]	SADABS[18]	SADABS[18]
reflns measured	20923	13683	15245	15694
unique reflns (R_{int})	6711	4065	5061	5159
reflns $I > 2\sigma(I)$	5613	3268	4917	4934
R1 [$I > 2\sigma(I)$]	0.029	0.052	0.022	0.048
wR2	0.067	0.119	0.050	0.130
GOF	1.055	1.775	1.113	1.623

[a] Crystallographic data for compounds **3** and **4** are given in tables of the Supporting Information. [b] The polarity of the crystal was determined with the Flack parameter of 0.02(2) (Flack, H. D. *Acta Crystallogr.* **1983**, *A39*, 876−881).

In all cases, "dark" (before irradiation) and "light" (after irradiation) data were collected on the same crystal. Identical collection and integration procedures were used. Crystallographic data for compounds **5** and **6** are presented in Table 1, while those for **3** and **4** are given in Tables S1 and S5 of the Supporting Information.

Table 2. Selected Experimental and Theoretical Bond Lengths (Å) and Angles (deg) for the *trans*-$Ru(NH_3)_4(SO_2)(H_2O)^+$ Cation (**5**)

	expt		theory[a]		
	GS	MS2	GS	MS2	MS1
Ru1−S1(O_2)	2.0892(5)	2.365(8)	2.104	2.414	N/A
Ru1−O1(SO)	N/A	2.08(2)	N/A	2.063	1.954
Ru1−O3(trans)	2.129(1)	2.03(2)	2.162	2.098	2.098
Ru1−N(eq)	2.126(2)	2.14(2)	2.126	2.132	2.119
	2.109(2)	2.09(2)	2.113	2.104	2.114
	2.115(2)	2.10(2)	2.127	2.121	2.109
	2.116(2)	2.11(2)	2.115	2.112	2.105
S1−O1	1.437(2)	1.49(2)	1.447	1.543	1.524
S1−O2	1.442(2)	1.44(2)	1.446	1.459	1.461
∠OSO	116.06(9)	127(1)	120.2	114.2	112.8
∠NRuSO	28.86(9)	35.2(9)	12.8	26.8	6.4
ν_{symm}(SO), cm^{-1}	1126	944	1140	934	945
ν_{asymm}(SO), cm^{-1}	1283	1180	1281	1208	1206

[a] Theoretical data are for the basis set 2 taken from ref 9.

Table 3. Selected Experimental and Theoretical Bond Lengths (Å) and Angles (deg) for the *trans*-$Ru(NH_3)_4(SO_2)(CF_3COO)^+$ Cation (**6**)

	expt		theory		
	GS	MS2	GS	MS2	MS1
Ru1−S1(O_2)	2.0945(5)	2.326(5)	2.104	2.338	N/A
Ru1−O1(SO)	N/A	2.07(1)	N/A	2.093	1.966
Ru1−O3(trans)	2.084(2)	2.09(1)	2.059	2.022	2.016
Ru1−N(eq)	2.105(2)	2.17(1)	2.106	2.12	2.102
	2.123(2)	2.14(1)	2.106	2.10	2.103
	2.127(2)	2.16(1)	2.106	2.11	2.106
	2.121(2)	2.13(1)	2.106	2.08	2.108
S1−O1	1.444(2)	1.50(1)	1.452	1.540	1.523
S1−O2	1.446(2)	1.42(1)	1.458	1.474	1.476
C1−O3	1.265(2)	1.29(1)	1.281	1.285	1.284
C1−O4	1.228(3)	1.22(1)	1.227	1.225	1.226
C1−C2	1.547(3)	1.61(1)	1.539	1.539	1.537
C2−F	1.340(2)	1.34(2)	1.334	1.332	1.334
	1.328(3)	1.31(1)	1.313	1.313	1.314
	1.335(3)	1.39(2)	1.334	1.335	1.335
∠OSO	114.5(1)	119.0(6)	118.2	115.1	112.6
∠NRuSO	−8.9(1)	36.3(5)	43.7	3.2	40.6

Differential Scanning Calorimetry (DSC). A Perkin-Elmer differential scanning calorimeter DSC7 was used for the DSC experiments. To maintain good temperature control, the sample cavity was continuously purged with ultrapure He gas. To minimize moisture in the system, the cold reservoir was flushed with N_2 gas. After at least 30 min exposure of 5−10 mg crystalline samples by 488 nm light from an Ar^+ laser, and a delay of 10−20 min for thermal equilibration, the samples were heated at a constant rate of 4°/min starting from 100 K, as the enthalpy supplied for the heating was being monitored.

Infrared Spectroscopy. FT-IR experiments were performed on a BioRad FTS40A IR spectrometer equipped with an MCT detector. An APD Helitran LT-3-110 optical cryostat equipped with NaCl windows and connected to a liquid nitrogen tank was used to cool the samples to 90 K. Freshly prepared KBr pellets (approximately 1 mm thick) were mounted in an IR transmission cell. The cell was mounted in the cryostat and evacuated to approximately 10^{-7} bar using a turbo-molecular pump. The temperature of the sample was controlled to within 1 K using a Scientific Instruments temperature controller (9620-R-1-1). The sample was irradiated in situ at 90 K for approximately 15−20 min with light from a 300 W Xe arc lamp passed through a heat absorbing water filter and a 350−550 nm broadband filter. Samples were mounted at 45° to both the IR beam and the irradiating light. Spectral resolution was 1 cm^{-1}.

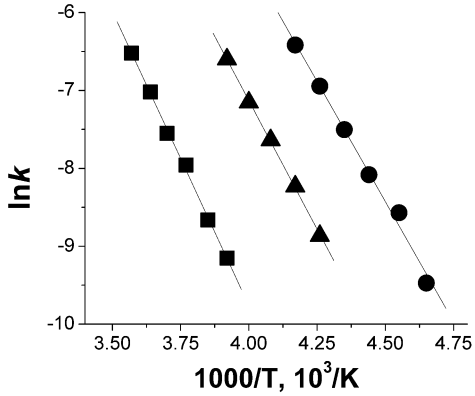

Figure 2. Arrhenius plots for compounds **3** (●), **5** (■), and **6** (▲). The solid lines show linear fits to the experimental points.

To obtain kinetic data on the decay of the metastable species, IR spectra of the irradiated samples were measured as a function of time at different temperatures. After irradiation, each sample was warmed to the selected temperature, and 7−10 spectra were collected at fixed time intervals. Temperature ranges 215−240, 255−280, and 235−255 K with 5 K steps were used for compounds **3**, **5**, and **6**, respectively.

Plots of the natural logarithm of the maximum absorbance versus time at each temperature are linear, indicating first-order kinetics of the MS2-to-GS (ground-state) thermal back reaction, and allowing determination of the rate constant *k*. Kinetics data could not be obtained for compound **4** as the SO_2 bands are not clearly resolved. Plots of ln *k* versus T^{-1} for compounds **3**, **5**, and **6** are shown in Figure 2 and discussed further in a following section.

Theoretical Calculations. All calculations were performed with the GAUSSIAN98 package[20] using density functional theory (DFT) with the local density approximation (LDA) in the parametrization of Vosko, Wilk, and Nusair (VWN5).[21] The effective core potential (ECP) LANL2DZ set was used for the ruthenium atom. An extended triple-ζ 6-311++G(2df,2pd) basis set was used for C, N, O, S, and F atoms and a 6-31+G** set for the H atoms. All molecular geometries were optimized without symmetry restrictions. Convergence criteria of 10^{-6} (au) for the density matrix, 4.5×10^{-4} (au/Å) for the gradients, and 1.8×10^{-3} (Å) for the displacements were used. All calculations were spin-restricted.

Results

Ground-State Structures. The structures were solved by using either the Patterson method (**3** and **4**) or direct methods (**5** and **6**). They were subsequently refined by full-matrix least-squares with anisotropic temperature parameters for all non-hydrogen atoms. Hydrogen atoms were located in the difference Fourier maps. The NH_3 ligands were refined as idealized groups with $U_{iso}(H) = 1.5U_{eq}$ of the nitrogen atom and were allowed to rotate around the N−Ru bonds during the refinement. The positions of hydrogen atoms of the water molecules in complexes **4** and **5** were refined independently with U_{iso} fixed at 1.5 U_{eq} of the O atom. The aromatic H atoms in **5** were refined with the riding model. Crystallographic data and final positional, isotropic temperature, and anisotropic displacement parameters together with bond lengths and angles are listed in Table 1 and in the tables of

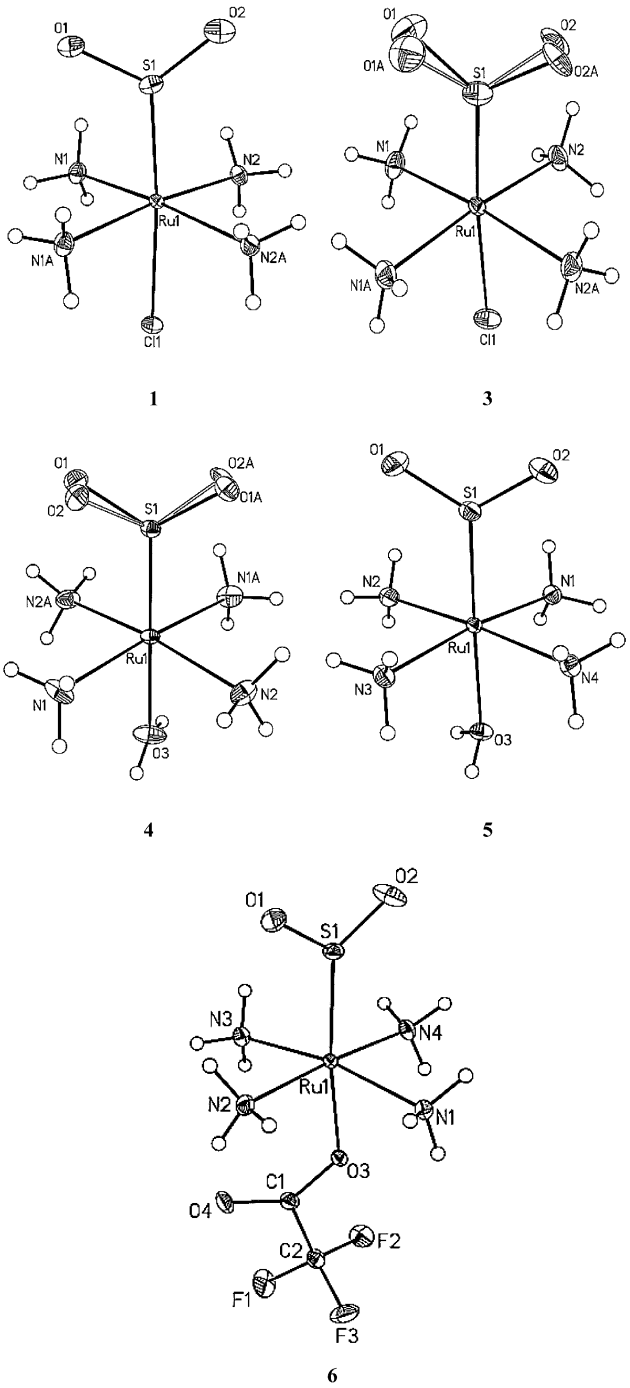

Figure 3. Ground-state geometry of the cations of **1** (from ref 9) and **3**−**6** and numbering of the atoms. Probability ellipsoids (50%) are shown. Atoms N1A and N2A in **3** are related to N1 and N2 by the crystallographic mirror plane. Atoms N1A and N2A in **4** are related to N1 and N2 by the rotation around the crystallographic 2-fold axis through the S1, Ru1, O3 molecular axis.

(20) Frisch, M. J.; Trucks, G. W.; Schlegel, H. B.; Scuseria, G. E.; Robb, M. A.; Cheeseman, J. R.; Zakrzewski, V. G.; Montgomery, J. A., Jr.; Stratmann, R. E.; Burant, J. C.; Dapprich, S.; Millam, J. M.; Daniels, A. D.; Kudin, K. N.; Strain, M. C.; Farkas, O.; Tomasi, J.; Barone, V.; Cossi, M.; Cammi, R.; Mennucci, B.; Pomelli, C.; Adamo, C.; Clifford, S.; Ochterski, J.; Petersson, G. A.; Ayala, P. Y.; Cui, Q.; Morokuma, K.; Malick, D. K.; Rabuck, A. D.; Raghavachari, K.; Foresman, J. B.; Cioslowski, J.; Ortiz, J. V.; Stefanov, B. B.; Liu, G.; Liashenko, A.; Piskorz, P.; Komaromi, I.; Gomperts, R.; Martin, R. L.;Fox, D. J.; Keith, T.; Al-Laham, M. A.; Peng, C. Y.; Nanayakkara, A.; Gonzalez, C.; Challacombe, M.; Gill, P. M. W.; Johnson, B. G.; Chen, W.; Wong, M. W.; Andres, J. L.; Head-Gordon, M.; Replogle, E. S.; Pople, J. A. *Gaussian 98*, Gaussian, Inc.: Pittsburgh, PA, 1998.
(21) Vosko, S. H.; Wilk, L.; Nusair, M. *Can. J. Phys.* **1980**, *58*, 1200−1211.

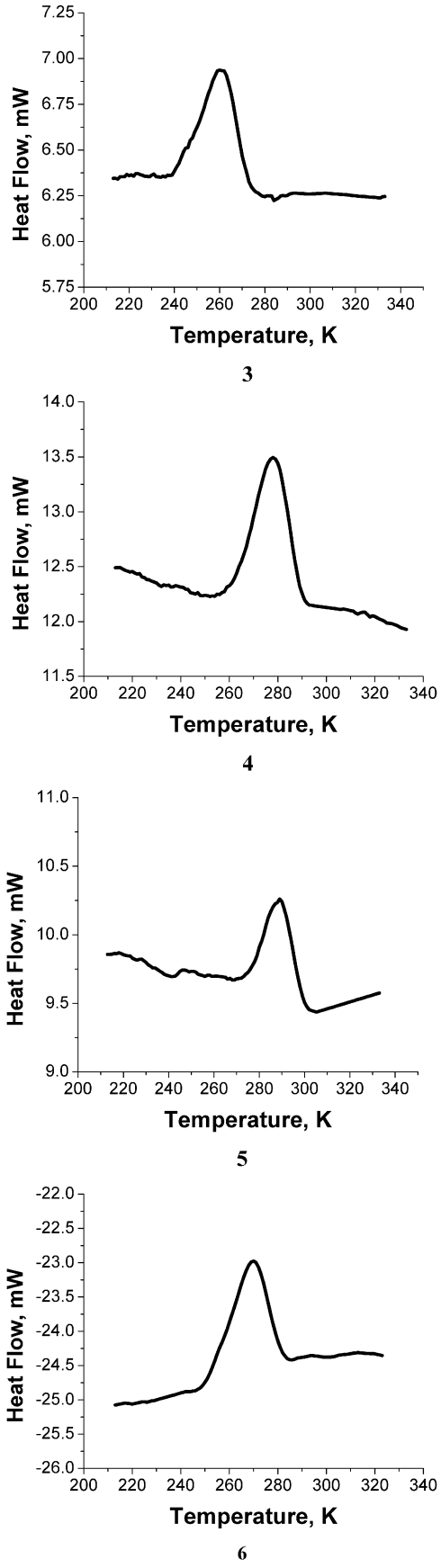

Figure 4. Heat flow vs temperature, for a constant temperature increase of 4 K/min, of a previously laser-irradiated single-crystal sample of **3**−**6**. The difference between the dark and illuminated sample curves is shown. Zero of the vertical scale is arbitrary.

the Supporting Information. The molecular structures are illustrated in Figure 3.

DSC Experiments and MS2 Structures. The difference DSC curves of irradiated crystals of complexes **3**−**6** are shown in Figure 4. The light-induced metastable states show the maximal decay rates at 261, 278, 289, and 270 K for compounds **3**, **4**, **5**, and **6**, respectively.

In the initial refinement, all atoms were located at the ground-state positions. The fractional coordinates of the GS structure were adjusted to account for slight differences between the unit cell dimensions from the "dark" and "light" experiments, such that the geometry of the GS molecule was as in the GS structure and the cation located at the center of mass of the GS structure. Refinement of only the scale factor yielded agreement factors of R1 = 0.174, wR2 = 0.367 for **5** and R1 = 0.164, wR2 = 0.402 for **6**. Photodifference maps using the scale factor from the refinement showed light-induced residual features similar to those observed for *trans*-$[Ru(NH_3)_4Cl(SO_2)]Cl$ and *trans*-$[Ru(NH_3)_4(H_2O)(SO_2)](C_6H_5SO_3)_2$,[9] with maximum/minimum values of 16.0/−8.3 e/Å^3, at 0.45 Å from the position of the Ru atom and 0.08 Å from the position of S1, respectively, in complex **5**, and 15.6/−3.4 e/Å^3, at 0.32 Å from the position of the Ru atom and 1.01 Å from the position of H3B, respectively, in complex **6**. As in our previous study,[9] the locations of the light-induced peaks are in agreement with an η^1-*S*-planar-to-η^2-*S*,*O*-side-bound linkage isomerization of the sulfur dioxide ligand.

The subsequent least-squares refinement of the metastable state MS2 was carried out as described previously.[1,7,9] The expression for the structure factor *F* of the crystal containing both ground and metastable states, assuming a random distribution of the metastable molecules in the crystal, is

$$F = (1 - P)F_{GS} + PF_{MS} + F_{rest}$$

where GS and MS indicate the ground and metastable states, respectively; P is the metastable state population, while the subscript rest represents any component of the crystal not involved in the excitation.

The MS2 populations of the cations of **5** and **6** were refined to 20.1(4)% and 37.3(5)%, respectively. In the subsequent refinement cycles, positional and isotropic thermal parameters of MS2 (anisotropic for Ru1 and S1 atoms in **5**, and for Ru1, S1 and O3 in **6**) were refined, while in a single cycle, the GS molecule was allowed to move as a rigid body (changes in atomic positions were less than 0.002 Å), to give R1 = 0.049 and wR2 = 0.113 for compound **5**, and R1 = 0.048 and wR2 = 0.130 for compound **6**. The highest remaining maximum and deepest electron density minimum in the difference Fourier synthesis were 1.42 e/Å^3 (1.04 Å from the position of S1 atom of the MS2) and −1.11 e/Å^3 (0.43 Å from the position of S1 atom of the GS), respectively, for complex **5**, and 1.91 e/Å^3 (0.47 Å from the position of O1 atom of the GS) and −1.75 e/Å^3 (0.07 Å from the position of O1 atom of the MS2), respectively, for complex **6**. In our experience, such residual electron density peaks are not significant in this kind of analysis and do not correspond to an additional species in the crystals.

Table 4. Comparison of Selected Experimental and Theoretical GS and MS2 Structural Parameters (Å and deg) in the Ru−SO_2 Complexes

GS Experiment					
complex	Ru−S	Ru−X	S−O	X−Ru−S	∠NRuSO
1	2.080(1)	2.407(1)	1.451(3) 1.426(4)	175.57(4)	44.55(7)
2	2.0853(4)	2.101(2)	1.448(1) 1.446(1)	178.56(5)	−26.98(8)
3	2.085(2)	2.395(2)	1.465(7) 1.444(7)	175.22(7)	−26.1(3) 32.1(3)
4	2.0899(8)	2.141(3)	1.452(5)[a] 1.428(5)[a]	180	−27.6(2) 52.0(2)
5	2.0892(5)	2.128(1)	1.441(2) 1.437(2)	178.14(4)	28.86(9)
6	2.0945(5)	2.084(2)	1.446(2) 1.444(2)	172.95(4)	13.7(1)
GS Theory (DFT)					
1, **3**	2.114	2.338	1.457 1.457	180	−23.4
2, **4**, **5**	2.104	2.162	1.447 1.446	180	12.8
6	2.104	2.059	1.458 1.452	177.1	43.7

MS2 Experiment										
complex	Ru−S	Ru−O	S−O	ΔRu−X	X−Ru−S	X−Ru−O	SO_2/eq	SORu/RuX	∠NRuSO	conversion %
1	2.32(2)	2.19(3)	1.46(3) 1.41(6)	−0.08(1)	150.1(5)	172.3(9)	21	180	49.3(8)	10.0(1)
2	2.401(8)	2.38(2)	1.51(2) 1.45(2)	−0.02(2)	160.7(5)	162.6(6)	13	180	39.2(8)	11.1(1)
5	2.365(8)	2.08(2)	1.49(2) 1.44(2)	−0.10(2)	165.0(5)	155.3(6)	21	175	35.2(9)	20.1(4)
6	2.326(5)	2.07(1)	1.50(1) 1.42(1)	0.01(1)	153.9(3)	164.6(3)	23	173	36.3(5)	37.3(5)
MS2 Theory (DFT)										
1	2.373	2.124	1.534 1.473	−0.04	159.6	160.7	13	180	42.3	N/A
2, **5**	2.414	2.098	1.543 1.459	−0.06	155.4	165.2	17	180	26.8	N/A
6	2.338	2.093	1.540 1.474	−0.04	153.6	164.3	16	173.9	3.2	N/A

[a] Two SO bonds of SO_2 are related by symmetry; values are for the two conformations.

Final positional and thermal parameters and bond lengths and angles of the MS2 structures are listed in the Supporting Information. The geometries of the MS2 molecules of **5** and **6** are illustrated in Figure 6.

Discussion

Ground-State Structures (Figure 3, Tables 2 and 3). The complexes studied fall into three groups according to the trans-to-SO_2 ligand, which is chloride in **1** and **3**, water in **2**, **4**, and **5**, and trifluoroacetate in **6**. Compounds **3** and **4** share the BF_4 counterion, while the anions differ in the other complexes. Selected experimental and theoretical geometric parameters are compared in Table 4. The ground-state geometries are reasonably well reproduced by the calculations, except for the Ru−X bonds for which discrepancies of ≈0.06 Å are found for the *trans*-Cl and *trans*-H_2O cations.[9]

In **3**, the crystallographic mirror plane of the *Pnma* space group bisects two of the N−Ru−N angles. In all complexes, except **4**, in which it is restricted to 180° by the crystallographic 2-fold axis, the X−Ru−S angle deviates from 180°. The deviation is largest in **6**, in which the bulky TFA ligand contributes to the distortion, as confirmed by the nonlinearity of the theoretical structure for the isolated complex. But the X−Ru−S group is calculated to be linear in the H_2O and Cl substituted cations, indicating that the observed deviations in these complexes are due to crystal forces.

In **3** and **4**, sulfur dioxide is disordered over two positions related by rotation around the Ru−S bond. The N−Ru−S−O angle, listed in Table 4, shows quite a large range of values. In **6**, which crystallizes in the noncentrosymmetric space group *Cc*, the sulfur dioxide plane is almost eclipsed with two of the Ru−N bonds, with a N4−Ru1−S1−O2 torsion angle of −8.9(1)°. Theoretical calculations show that the barrier for SO_2 rotation around the Ru−S bond is very small. It was calculated for the *trans*-H_2O ion using partial optimization, with the N−Ru−S−O angles fixed at values ranging from 0° to 180°. The rotation barrier is located at the staggered SO_2 conformation with the N−Ru−S−O torsion angle of 45° (Figure 5). Its height is only 1.7 kcal/mol, and thus, the barrier can be easily overcome at room temperature in the free molecule, or in a molecule in solution. Thus, the SO_2 conformation will be affected by crystal packing forces, in agreement with the range of values for the N−Ru−S−O torsional angle listed in Table 4.

The sulfur dioxide S−O bonds show small differences

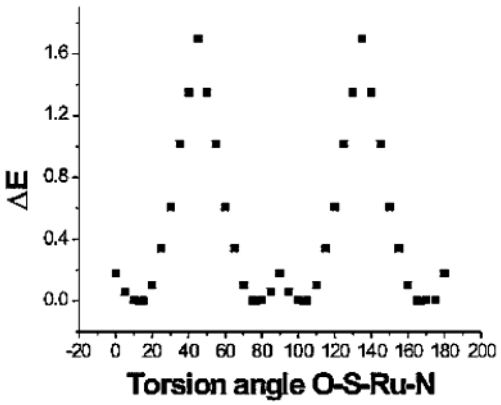

Figure 5. Calculated potential curve for rotation of the SO_2 group around the Ru−S bond in the $[Ru(NH_3)_4(SO_2)(H_2O)]^{2+}$ ion. For details of the calculation, see text. All geometric parameters except the N−Ru−S−O angle have been optimized at each point in the figure.

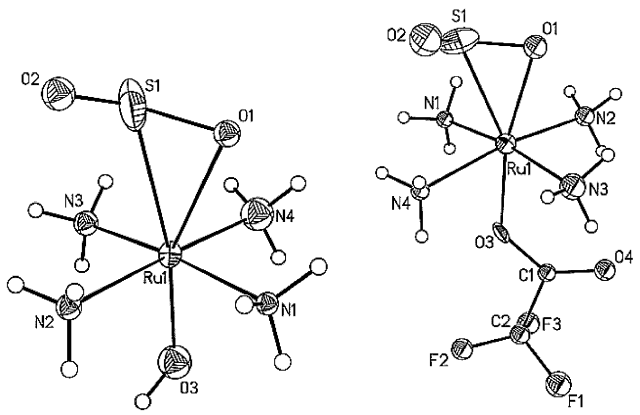

Figure 6. Geometry of the cation of **5** and **6** in the metastable state MS2 and numbering of atoms. Probability ellipsoids (50%) are shown.

within each complex, which are not reproduced by the calculations, and may similarly be attributed to intermolecular interactions in the crystal.

While the water molecule is planar bound to the ruthenium in **2** and **4**, it is pyramidally bound in tosylate complex **5**. According to theory, the cation with the planar water coordination corresponds to the global minimum on the potential energy surface, whereas the pyramidal coordination is destabilized by 3.6 kcal/mol. In the crystal of **5**, the latter coordination is stabilized by strong O−H···O−S(O_2) hydrogen bonds with the neighboring tosylate ions. The distances H3(OA)···O9 and H3(OB)···O6 are 1.82(1) and 1.85(1) Å, respectively, and the angles O3−H3(OA)···O9 and O3−H3(OB)···O6 are 168(1)° and 174(1)°, respectively.

Light-Induced Metastable States (Figure 6, Table 4). Selected dimensions are listed in Table 4, together with the metastable state populations. It is evident that experimental standard deviations decrease with increased conversion, which is highest for TFA complex **6**. The experimental geometry changes upon isomerization include a shortening of the bonds between Ru and the axial ligand in **1** and **5**, which according to the isolated-molecule calculation occurs in all complexes. The Ru−N distances are essentially unchanged.

Table 5. FT-IR SO_2 Frequencies and Thermodynamic Quantities for Compounds **1**−**6**

	1	**2**	**3**	**4**	**5**	**6**
GS	1110	1126	1110	1111	1126	1122
ν, cm^{-1}	1253	1279	1257	1260	1283	1275
MS2	942	946	943	944	944	954
ν, cm^{-1}	1165	1181	1167	1163	1180	1164
T_d, K	230	262	235		276	252
E_a, kJ/mol	50.0	58.4	51.6		62.8	55.2
A, s^{-1}	2.6×10^8	4.5×10^8	2.5×10^8		7.6×10^8	2.7×10^8
$\Delta S^{\ddagger}$, J/mol·K	−90.0	−86.3	−90.5		−82.7	−90.3

Three noticeably different Ru−S−O coordination geometry types can be distinguished: (1) In **1** and **6**, the oxygen atom is closer to the molecular axis and to ruthenium than sulfur. (2) In **2**, oxygen and sulfur are symmetrically bound to the ruthenium, with ruthenium, sulfur, and oxygen located at the apices of an isosceles triangle. (3) In **5**, the sulfur atom is closer to the molecular axis than the oxygen, but further from Ru. The theory for the isolated species predicts type 1 for all three cations, again indicating that packing forces may affect the details of the conformation.

In all complexes, the orientation of the S−O bond of SO_2 with respect to the equatorial ligands is close to staggered, the torsion angle varying from ≈35−49°, though the calculated conformations show a greater variation. They are close to staggered (42.3°) in the case of the chloro-substituted cation, gauche (26.8°) in the aqua cation, and eclipsed (3.2°) in the trifluoroacetate cation. The sulfur dioxide plane in MS2 is inclined to the plane of the equatorial ligands by approximately 20° in all the cations, except for benzene sulfonate aqua complex **2** where it is 13°.

The quantum-chemical calculations indicate that not only an MS2 isomer but also an MS1 (η^1-*O*-bound, U-shaped) isomer correspond to local minima on the ground-state potential energy surface. The energy-optimized MS1 species shows no negative eigenvalues of the Hessian matrix (the matrix of the second derivatives of the potential energy surface) of the potential energy surface and thus have no imaginary frequencies.

The theoretical energy differences between the MS2 and GS states are small for the chloro-, aqua-, and trifluoroacetate-substituted $RuSO_2$ cations, whereas MS1 states tend to be considerably less stable than GS: MS2 is 3.2 kcal/mol (0.14 eV), 3.3 kcal/mol (0.142 eV), and 6.1 kcal/mol (0.27 eV) less stable than GS in chloro-, trifluoroacete-, and aqua-substituted cations, respectively, the corresponding values for MS1 being 12.7 kcal/mol (0.55 eV), 13.7 kcal/mol (0.596 eV), and 5.4 kcal/mol (0.24 eV). The increase in stability of the aqua-substituted MS1 state relative to those of the other two cations is due to the formation of an intramolecular hydrogen bond between the terminal SO_2 oxygen and a hydrogen atom of the closest NH_3 group.[9]

Infrared Spectroscopy. IR spectroscopic data are summarized in Table 5. As expected, GS SO_2 stretching vibrations are similar in all complexes and range from 1110 to 1126 cm^{-1} and from 1253 to 1283 cm^{-1} for the symmetric and asymmetric vibrations, respectively. Light exposure of the KBr pellets at 90 K causes a bleaching of these bands, while bands corresponding to the η^2-side-bound SO_2 ligand

Table 6. MS2 Decay Rate Constants for Compounds **3**, **5**, and **6** from IR Data

T, K	*k*, 10^{-3} s^{-1}	*T*, K	*k*, 10^{-3} s^{-1}	*T*, K	*k*, 10^{-3} s^{-1}
215	0.077	255	0.106	235	0.141
220	0.190	260	0.173	240	0.266
225	0.309	265	0.355	245	0.482
230	0.551	270	0.526	250	0.782
235	0.963	275	0.893	255	1.360
240	1.630	280	1.470		

of MS2 appear in the range 942−954 cm^{-1} for the symmetric SO_2 vibration and 1163−1181 cm^{-1} for the asymmetric SO_2 vibration. The downshift is similar to that observed for the side-bound nitrosyl and dinitrogen complexes.[8]

The thermal decay of the MS2 IR bands follows first-order kinetics (Table 6). The rate constants *k* for the reaction at each temperature can be derived from the absorbance versus time plots. The Arrhenius equation

$$\ln k = -(E_a/RT) + C$$

where *R* is the molar gas constant and *C* is the natural logarithm of the frequency factor (*A*) has been used to calculate the activation energy of the reaction and frequency factors, which are listed in Table 5. Entropy of activation values were obtained with the Eyring equation

$$k = (k_B T/hC) \times \exp(\Delta S^{\ddagger}/R) \times \exp(-\Delta H^{\ddagger}/RT)$$

where k_B is the Boltzman constant, *h* is the Planck constant, *C* equals unity, *R* is the molar gas constant, $\Delta S^{\ddagger}$ is the entropy of activation, and $\Delta H^{\ddagger}$ is the enthalpy of activation, by plotting ln(*k*/T) versus 1/*T* with slope $\Delta H^{\ddagger}/R$, and intercept at $T = \infty$ equal to $\Delta S^{\ddagger}/R + \ln(k_B/h)$.

Figure 2 shows the Arrhenius plots for compounds **3**, **5**, and **6**. Using the definition of the decay temperature (T_d) of a metastable state as the temperature at which the rate constant for the thermal decay of the light-induced species is 10^{-3} s^{-1}, proposed by Morioka et al.,[22] T_d values were calculated for all compounds (Table 4), except **4**, which on irradiation shows two overlapping pairs of light-induced bands (944, 1163 cm^{-1} and 950, 1190 cm^{-1}), both in the region of sulfur dioxide stretching bands. The first pair (944, 1163 cm^{-1}) does not start to decay significantly up to about 250−255 K, whereas the second (950, 1190 cm^{-1}) already decays rapidly at about 220−230 K. Because of the overlapping of these IR bands, neither T_d nor E_a could be calculated. The frequencies of these bands and their relative decay rates suggest that the slower decaying 944, 1163 cm^{-1} pair corresponds to MS2, whereas the second pair could possibly be due to the generation of the MS1, η^1-*O*-bound isomer predicted by the calculations.

As can be seen in Table 5, the T_d increases from 230 K to 276 K in the sequence **1** < **3** < **6** < **2** < **5**, or *trans*-Cl < TFA < H_2O, which corresponds to the σ-electron donating ability of the *trans*-ligand, and in the case of **1** and **3**, and **2** and **5**, to the size of the counterions. Thus, the stronger the electron donating ability of the ligand (Lewis basicity) and the larger the counterion, the higher T_d of the MS2 isomer. The activation energies increase in the same order as the decay temperatures from 50.0 kJ/mol for complex **1** to 62.8 kJ/mol for complex **5**. These values are comparable with and slightly larger than the activation energies for nitrosyl linkage isomers determined by DSC and IR measurements,[23−25] as may be expected for the sterically larger SO_2 ligand. Such dependence of T_d on the Lewis basicity of the trans-to-SO_2 ligand can be explained in terms of the electronic structure of the M−SO_2 bond. When sulfur dioxide is planar S-bound to a d^6 metal (like Ru^{II}), the M−SO_2 bond is mainly due to σ-electron donation from the lone electron pair of sulfur to the empty d_{z^2} metal orbital. The degree of π-back-donation to the π^* of SO_2 is much less. On the other hand, π-back-donation becomes significant in the η^2-*S*,*O*-binding mode. Therefore, a better Lewis base trans-to-SO_2 which increases the electron density on the metal can increase the π-back-donation to the SO_2 ligand and, thus, stabilize the MS2 isomer.

Concluding Remarks

Photoinduced linkage isomerism is clearly quite common in $Ru^{II}SO_2$ complexes. The thermal stability of the metastable states can be increased by increasing the σ-donating ability of the trans ligand and by increasing the size of the counterion. It is quite plausible that room-temperature stable MS2-type isomers, useful for erasable memory applications, do exist. There is some indication in the spectra for the existence of the theoretically predicted, but less stable, MS1-type isomer, the formation of which may be hampered by space restrictions in the crystal matrix. Inclusion of the complex in the cavities of supramolecular solids may relieve the packing restrictions and allow observation of such species.

Acknowledgment. Financial support of this work by the National Science Foundation (CHE9981864) and the Petroleum Research Fund of the American Chemical Society (PRF32638AC3) is gratefully acknowledged. J.M.C. also wishes to thank the Royal Society of Chemistry for a Journals Grant (00 06/257) and St. Catharine's College, Cambridge, U.K., for a Bibby Research Fellowship.

Supporting Information Available: Crystallographic data in CIF format and additional tables. This material is available free of charge via the Internet at http://pubs.acs.org.

IC025997G

(22) Morioka, Y.; Ishikawa, A.; Tomizawa, H.; Miki, E. *J. Chem. Soc., Dalton Trans.* **2000**, 781−786.

(23) Zöllner, H.; Woike, T.; Krasser, W.; Haussühl, S. *Z. Kristallogr.* **1989**, *188*, 139.

(24) Woike, T.; Zöllner, H.; Krasser, W.; Haussühl, S. *Solid State Commun.* **1990**, *73*, 149−152.

(25) Woike, T.; Haussühl, S. *Solid State Commun.* **1993**, *86*, 333−337.